Published in final edited form as:
Opt Express. 2009 March 2; 17(5): 4208–4220.

Visualization of 3D high speed ultrahigh resolution optical coherence tomographic data identifies structures visible in 2D frames◊

Larry Kagemann[1,2], **Hiroshi Isikawa**[1,2], **Gadi Wollstein**[1], **Michelle Gabriele**[1,3], and **Joel S. Schuman**[1,3,*]

[1]UPMC Eye Center, Eye and Ear Institute, Ophthalmology and Visual Science Research Center, University of Pittsburgh School of Medicine, Pittsburgh, Pennsylvania, USA

[2]Department of Bioengineering, Swanson School of Engineering, University of Pittsburgh, Pittsburgh, Pennsylvania, USA

[3]Center for the Neural Basis of Cognition Carnegie Mellon University and University of Pittsburgh, Pittsburgh, Pennsylvania, USA

Abstract

Optical coherence tomography has allowed unprecedented visualization of ocular structures, but the identity of some visible objects within slices remains unknown. This study reconstructs a number of those objects in 3D space, allowing their identification by observation of their 3D morphology. In the case mottling deep within image slices through the optic disc, C-mode imaging provided visualization of the appearance and distribution of laminar pores. In the case of white spots and streaks sometimes observed in image slices through the cornea, C-mode imaging contoured to the path of those white spots allowed their visual identification as nerves extending radially into the cornea from the limbus. White spots observed in ultrahigh resolution retinal image slices were identified as blood within retinal capillaries. C-mode contour-corrected imaging of three-dimensional structures provided the identification of previously unidentified structures visible in cross-sectional image slices.

1. Introduction

Time domain optical coherence tomography (OCT) has applied interferometry for the non-invasive quantification of reflectance in ocular tissues [1-5]. Recent OCT technology has taken advantage of the characteristic of frequency encoding of depth information within the interference of broadband low coherence light [6,7]. Use of a spectrometer to capture the interferometric fringe pattern has greatly increased sensitivity and yielding a higher data acquisition rate of spectral domain high speed ultrahigh resolution spectral-domain optical coherence tomography (SdOCT) systems, and the availability of wide bandwidth light sources has improved axial resolution [8-11]. Figure 1 shows a horizontal cross-sectional B-scan image of the macula of a subject using the commercially available time domain OCT system, and a similar slice from the same eye obtained with an SdOCT system.

◊**Datasets associated with this article are available at** http://hdl.handle.net/10376/1220.

*Corresponding author: SchumanJS@UPMC.edu.

The increased axial resolution of SdOCT technology has provided better distinction of the various cell layers within ocular structures, but has also revealed microstructures that were previously unseen in OCT images (Fig. 2).

C-mode imaging is a well established technique for the visualization of 3D data sets produced by both time domain, and spectral domain OCT [12-15]. In contrast to the 400 A-scans per second scan rate of time domain OCT, the high acquisition rate of SdOCT allows the rapid acquisition of a series of frames in a raster pattern, creating a three-dimensional (3D) cube of reflectance data (Fig. 3). The device used in this study had a scan rate of 28,000 A-scans / second, though SdOCT scan rates currently vary from 25,000 to 250,000 A-scans / second.

Acquisition of 3D data may allow visualization of the morphology *in-situ*. The purpose of the present study was to reconstruct in 3D space, and subsequently identify unknown microstructures visualized by SdOCT.

2. Methods

2.1 Ethical considerations

Imaging was performed in two normal healthy subjects at the University of Pittsburgh Medical Center (UPMC) Eye Center. Both subjects had no history or evidence of intraocular surgery, retinal disease, glaucoma, or refractive error greater than ± 3 diopters. Both subjects had normal-appearing optic nerve heads and visual fields. Institutional review board and ethics committee approval was obtained for the study, and informed consent was obtained. This study followed the tenets of the Declaration of Helsinki and was conducted in compliance with the Health Insurance Portability and Accountability Act.

2.2 Imaging platform

Imaging was performed with a SdOCT consisting of an eye scanner and optics engine (Bioptigen Inc., Research Triangle Park, NC) coupled with a 4 diode 200nm bandwidth (centered at 870nm) broad band superluminescent diode (Q-870, Superlum, Co. Cork, Ireland). The theoretical limit for axial resolution in air (the coherence length of the light source) is a function of light source bandwidth and center wavelength as

$$\text{Axial Resolution} = \frac{2\ln(2)}{\pi} \cdot \frac{\text{center wavelength}^2}{\text{bandwidth}} \approx 0.4413 \cdot \frac{\text{center wavelength}^2}{\text{bandwidth}},$$

yielding a theoretical axial resolution of 1.7μm in air. Correcting for the index of refraction, the axial resolution in tissue is approximately 1.31μm. Actual resolution does not achieve the theoretical because of dispersion.

The scan protocol varied from 128 × 128 to 300 × 300 A-scans, depending on the tissue examined. Transverse scan areas varied from 4 × 4 mm to 0.8 × 0.8mm respectively. Each A-scan was 2 mm in depth.

2.3 Image processing

Images were processed in two steps. First, we used software of our own design (HI) to align retinal images such that the epiretinal membrane (first highly reflective surface encountered when the scanning beam moves posteriorly through the retina) was located on a flat line in the center of the image. This was accomplished by translating a-scans in the Z-direction. In the case of corneal images, alignment was made to the tear film. Next, thin transverse planes

within the aligned dataset were isolated, and reflectance values from those planes displayed as C-mode images (Fig. 4). 3D structures located within the tissue planes were approximately adjacent within the dataset; thus the aligned data allowed 2D imaging their morphology.

In the case of the cornea, the C-mode plane was manually placed on visible structures that spanned the 3D dataset, but were not precisely parallel to the adjacent tissues.

2.4 Ocular structures to be identified

Four distinct structures, visible in B-scan SdOCT frames, were examined in 3D space utilizing structure-conformed C-mode slabs for morphological identification.

2.4.1 Inner/outer plexiform hyper-reflective particles—Within the plexiform layers, clusters of bright pixels can be observed scattered randomly throughout. Unlike speckle noise, which occurs randomly as a single bright pixel, these structures appear to represent brightly reflecting structures relative to the surrounding tissues. (Fig. 2B, upper arrows) It has been proposed that they may represent blood vessels [16], but determination is impossible by examination of cross-sectional images alone.

2.4.2 Sub-retinal mottle—There appears, below the sharp bright lines of the retinal pigment epithelium/photoreceptor complex, a region of black and white mottle contains the choriocapillaris and large choroidal vasculature [17-19] (Fig. 5). As the mottle fades slowly with depth, it is impossible to determine, within the SD-OCT frame, at what point structure fades to noise.

2.4.3 Posterior optic nerve head streaks—It is possible to focus on deep layers of the optic nerve head, revealing structures within the pre-laminar and lamina cribrosa regions (Fig. 6). The clinical utility of cross-sectional images of the lamina cribrosa remains unknown. Clinicians do use exposure of laminar pores to judge the extent of disease in glaucoma, and pore size remains a topic of interest in both clinical practice and basic research. Unfortunately, it is difficult to quantify pore size and position from single cross-sectional slices of tissue.

2.4.4 Corneal hyper-reflective particles—Corneal imaging reveals a plethora of stromal structures, but cross-sectional imaging is of limited use in their identification. For example, a sequence of adjacent cross-sectional images of the limbus and cornea show large hyper-reflective streak in the stroma (arrow, Fig. 7) which varies in length depending on location. It is possible that these streaks may represent a number of large structures, or a different portion of a single structure, but it is impossible to determine the exact morphological nature of these structures (or structure) using cross-sectional slices alone.

3. Results

3.1 Inner/outer plexiform hyper-reflective particles

When aligned, a series of adjacent C-mode slabs cutting through the inner and outer plexiform layers (Fig. 8) contain retinal capillaries (Fig. 9). This suggests that the hyper-reflective points observed in OCT frames (Fig. 2B) are cross-sections of the capillaries in those layers.

3.2 Sub-retinal mottle

Isolation of the sub-retinal structure within a C-mode slab reveals the vascular pattern associated with the choriocapillaris. The image has been black/white inverted for easier visualization of the structure (Fig. 10).

3.3 Posterior optic nerve head streaks

The C-mode slab through the deep optic nerve head provides visualization of pores through the lamina cribrosa (Fig. 11). Specifically, pore size, density, and distribution across the optic nerve head were all readily visible.

3.4 Corneal hyper-reflective particles

A C-mode slab was placed onto the hype reflective streak and the slab was then conformed to the stromal structure. With alignment of the C-mode slab, a continuous structure entering the cornea from the limbus was observed (Fig. 12). A second faint similar structure was also observed.

4. Discussion

In the present study, structures in retinal inner and outer plexiform layers, subretinal layer, optic nerve head, and cornea were all consistently identified by morphological identification utilizing planar projections of their three-dimensional structures. In the case of the retinal capillaries in the inner and outer plexiform layers, the finding may be counterintuitive to those experienced in retinal OCT imaging. In Fig. 2A on the nasal (upper right) optic nerve head, large vessels appear as black ovals. Indeed, blood moving in large vessels results in a loss of back-scattering signal due to fringe washout [20]. But in the present study, the slow moving blood within retinal capillaries produced a high intensity back-scatter signal relative to the surrounding tissue (Fig. 2 B, arrows). The fact that slow moving or stationary blood produces a strong OCT signal implies that the bright circle surrounding the black center of large blood vessels is slow moving blood near the vessel edge, and not the vascular lumen (Fig. 2).

In Fig. 10 (upper left), it appears that blood within the choriocapillaris did not create a reflective signal. The lack of reflectance may suggest that, similar to blood in large retinal vessels, the blood within the choriocapillaris is moving so fast that fringe washout renders back-scattered light immeasurable with the present system. Inverting the data volume black/white provides visualization of the lack of back-scattered light, yielding an image reminiscent of previous vascular casting studies of the choroid.

Cross-sectional imaging of laminar pores may be clinically useful in the future, but the subjective examination of laminar pore size and distribution is currently considered in the management of glaucoma. Figure 11 demonstrates that lamina cribrosa pores can be visualized by focusing deep within the optic nerve head, and isolating the layer within a C-mode slab. The distribution and size of pores within the lamina cribrosa are each more readily visible in the C-mode slab than in the optic disc photo, suggesting that visualization of pores located beneath nerve fiber tissues is feasible with SdOCT.

In the corneal image, a highly reflective structure (Fig. 7) is observed extending from the limbus into the cornea. (Fig. 12, top) Given the avascular nature of the cornea, it is possible that these are cornea nerves. The low intensity of the secondary structure was due to slight displacement from the location of the C-mode used. Slight anterior relocation of the C-mode slab caused a number of nerves not readily visible in the cross-sectional series to come into view (Fig. 12, bottom).

5. Conclusions

C-mode imaging is a well established technique for the visualization of 3D data sets produced by both time domain, and spectral domain OCT. In the present study, in the case of the lamina cribrosa, C-mode imaging provided visualization of appearance and distribution of laminar pores. In the cornea and retinal images, C-mode imaging of three-dimensional structures allows identification of visible structures in SdOCT cross-sectional images that were previously unidentified.

Acknowledgments

This research was supported in part by National Institutes of Health R01-EY13178-08, P30-EY008098; The Pittsburgh Foundation; The Eye and Ear Foundation (Pittsburgh, PA); and unrestricted grants from Research to Prevent Blindness.

References and links

1. Huang D, Swanson EA, Lin CP, Schuman JS, Stinson WG, Chang W, Hee MR, Flotte T, Gregory K, Puliafito CA, et al. Optical coherence tomography. Science 1991;254:1178. [PubMed: 1957169]
2. Huang D, Wang J, Lin CP, Puliafito CA, Fujimoto JG. Micron-resolution ranging of cornea anterior chamber by optical reflectometry. Lasers Surg Med 1991;11:419. [PubMed: 1816476]
3. Fercher AF, Hitzenberger CK, Drexler W, Kamp G, Sattmann H. In vivo optical coherence tomography. Am J Ophthalmol 1993;116:113. [PubMed: 8328536]
4. Hitzenberger CK, Drexler W, Dolezal C, Skorpik F, Juchem M, Fercher AF, Gnad HD. Measurement of the axial length of cataract eyes by laser Doppler interferometry. Invest Ophthalmol Vis Sci 1993;34:1886. [PubMed: 8491541]
5. Morgner U, Drexler W, Kartner FX, Li XD, Pitris C, Ippen EP, Fujimoto JG. Spectroscopic optical coherence tomography. Opt Lett 2000;25:111. [PubMed: 18059799]
6. Fercher AF, Hitzenberger CK, Kamp G, El-Zaiat SY. Measurement of intraocular distances by backscattering spectral interferometry. Opt Commun 1995;117:43.
7. Häusler G, Linder MW. ‘Coherence rada’ and ‘spectral rada’—new tools for dermatological diagnosis. J Biomed Opt 1998;3:21.
8. de Boer JF, Cense B, Hyle Park B, Pierce MC, Tearney GJ, Bouma BE. Improved signal-to-noise ratio in spectral-domain compared with time-domain optical coherence tomography. Opt Lett 2003;28:2067. [PubMed: 14587817]
9. Leitgeb R, Hitzenberger C, Fercher A. Performance of Fourier domain vs. time domain optical coherence tomography. Opt Express 2003;11:889. [PubMed: 19461802]
10. Nassif N, Cense B, Park BH, Yun SH, Chen TC, Bouma BE, Tearney GJ, de Boer JF. In vivo human retinal imaging by ultrahigh-speed spectral domain optical coherence tomography. Opt Lett 2004;29:480. [PubMed: 15005199]
11. Wojtkowski M, Leitgeb R, Kowalczyk A, Bajraszewski T, Fercher AF. In vivo human retinal imaging by Fourier domain optical coherence tomography. J Biomed Opt 2002;7:457. [PubMed: 12175297]
12. Podoleanu, AG.; Dobre, GM.; Webb, DJ.; Jackson, DA. En-face OCT imaging of the retina using path modulation introduced by the transversal scanning mirror. In: Fujimoto, J.; Patterson, M., editors. Advances in Optical Imaging and Photon Migration, Vol 21 of OSA Trends in Optics and Photonics (Optical Society of America, 1998). paper AMC4
13. Pircher M, Goetzinger E, Leitgeb R, Hitzenberger CK. Transversal phase resolved polarization sensitive optical coherence tomography. Phys Med Biol 2004;49:1257. [PubMed: 15128203]
14. Potsaid B, Gorczynska I, Srinivasan VJ, Chen Y, Jiang J, Cable A, Fujimoto JG. Ultrahigh speed spectral/Fourier domain OCT ophthalmic imaging at 70,000 to 312,500 axial scans per second. Opt Express 2008;16:15149. [PubMed: 18795054]

15. Srinivasan VJ, Adler DC, Chen Y, Gorczynska I, Huber R, Duker JS, Schuman JS, Fujimoto JG. Ultrahigh-speed optical coherence tomography for three-dimensional and en face imaging of the retina and optic nerve head. Invest Ophthalmol Vis Sci 2008;49:5103. [PubMed: 18658089]

16. Cense B, Chen TC, Nassif N, Pierce MC, Yun SH, Park BH, Bouma BE, Tearney GJ, de Boer JF. Ultra-high speed and ultra-high resolution spectral-domain optical coherence tomography and optical Doppler tomography in ophthalmology. Bull Soc Belge Ophtalmol 2006:123. [PubMed: 17265794]

17. Hong Y, Makita S, Yamanari M, Miura M, Kim S, Yatagai T, Yasuno Y. Three-dimensional visualization of choroidal vessels by using standard and ultra-high resolution scattering optical coherence angiography. Opt Express 2007;15:7538. [PubMed: 19547079]

18. Lee EC, de Boer JF, Mujat M, Lim H, Yun SH. In vivo optical frequency domain imaging of human retina and choroid. Opt Express 2006;14:4403. [PubMed: 19516592]

19. Yasuno Y, Hong Y, Makita S, Yamanari M, Akiba M, Miura M, Yatagai T. In vivo high-contrast imaging of deep posterior eye by 1-μm swept source optical coherence tomography and scattering optical coherence angiography. Opt Express 2007;15:6121. [PubMed: 19546917]

20. Yun SH, Tearney GJ, de Boer JF, Bouma BE. Motion artifacts in optical coherence tomography with frequency-domain ranging. Opt Express 2004;12:2977. [PubMed: 19483816]

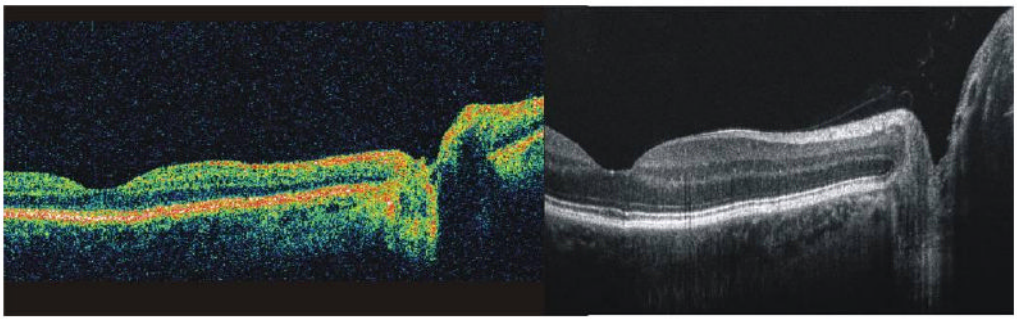

Fig. 1.
B-scans of the macula of a normal healthy eye imaged with OCT (left, fast macular scan, Stratus OCT®, Carl Zeiss Meditec, Dublin CA), and a SdOCT (right, Bioptigen, Inc., Research Triangle Park, NC).

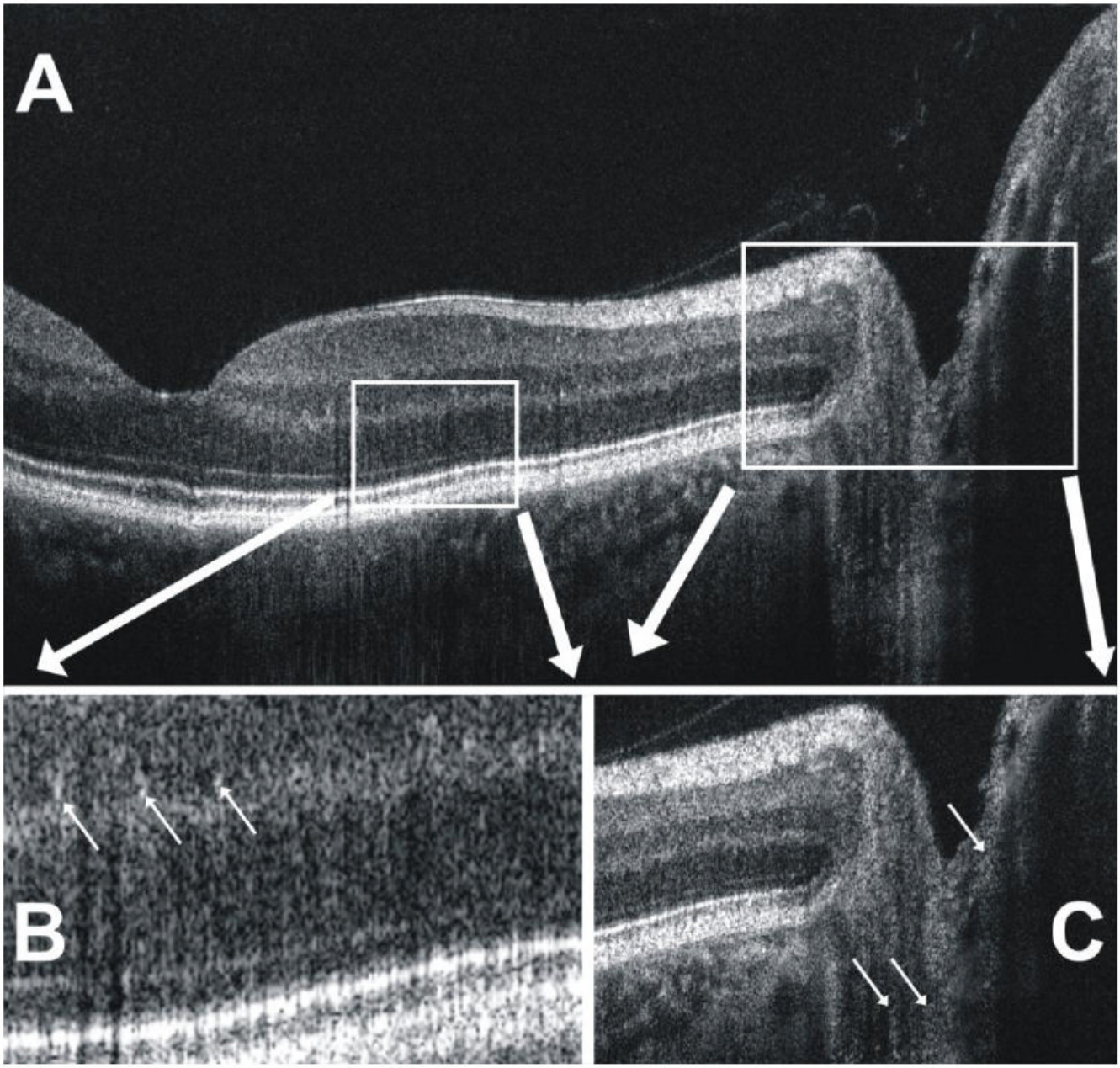

Fig 2.
(A) A closer look at the SdOCT B-scan image in Fig. 1 shows (B) the visualization of small white granular-appearing structures (arrows) in the inner and outer plexiform layers of the retina. (C) Similarly, faint structures appear (arrows) to be visualized in the posterior optic nerve head.

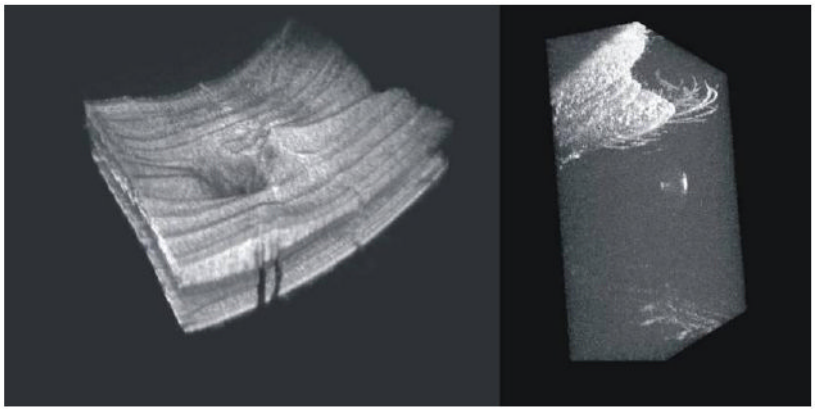

Fig. 3.
Projections of SdOCT 3D scans of peripapillary retina (left) and cornea and surrounding lids and eyelashes (right)

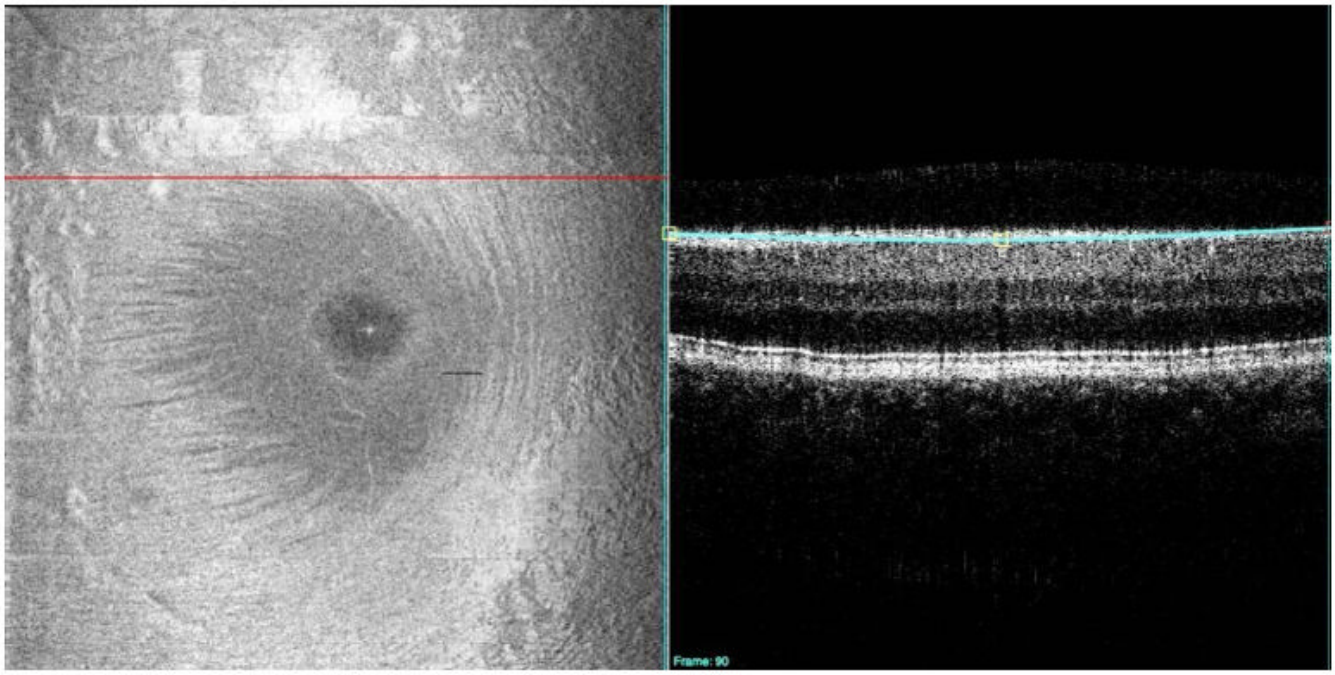

Fig. 4.

A C-mode image (left) contains an en-face view of a 3D dataset, but isolates reflection to a thin layer of tissue. In this figure, the thin blue line on the B-scan (right) shows the location of retinal nerve fiber layer imaged by C-mode on the left. The cross-sectional retinal B-scan slice (right) cuts through the retinal layers on a horizontal line superior to the macula (red line, left).

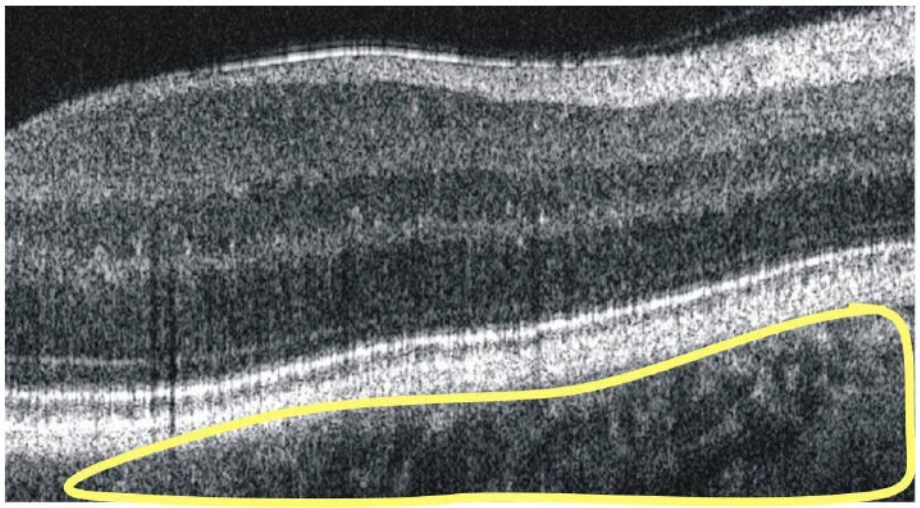

Fig. 5.
Choroidal and scleral structures are observed posterior to the retinal pigment epithelium/photoreceptor complex in a B-scan retinal image, and fade to noise in the deepest points of the image.

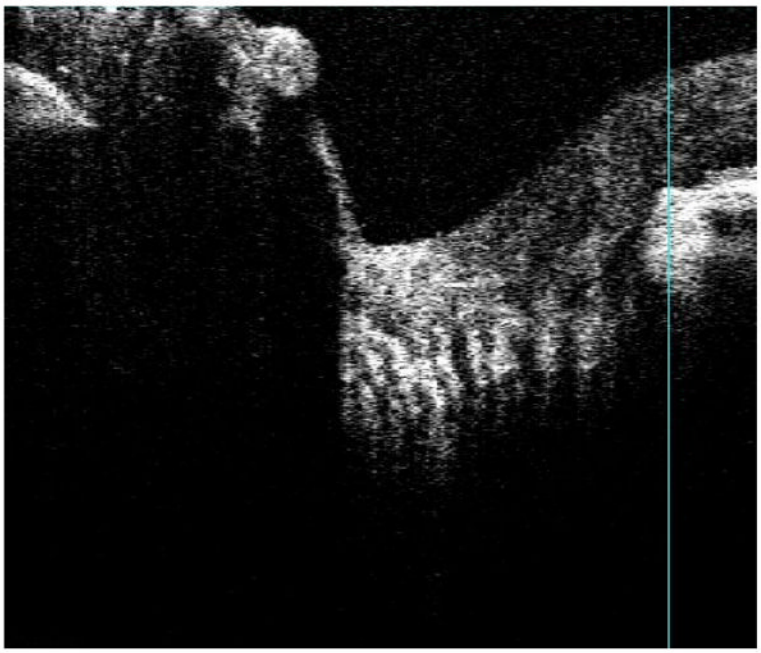

Fig. 6.
Focusing deep within the optic nerve head reveals pre-laminar and lamina cribrosa structures, observed here as vertical stripes in a B-scan.

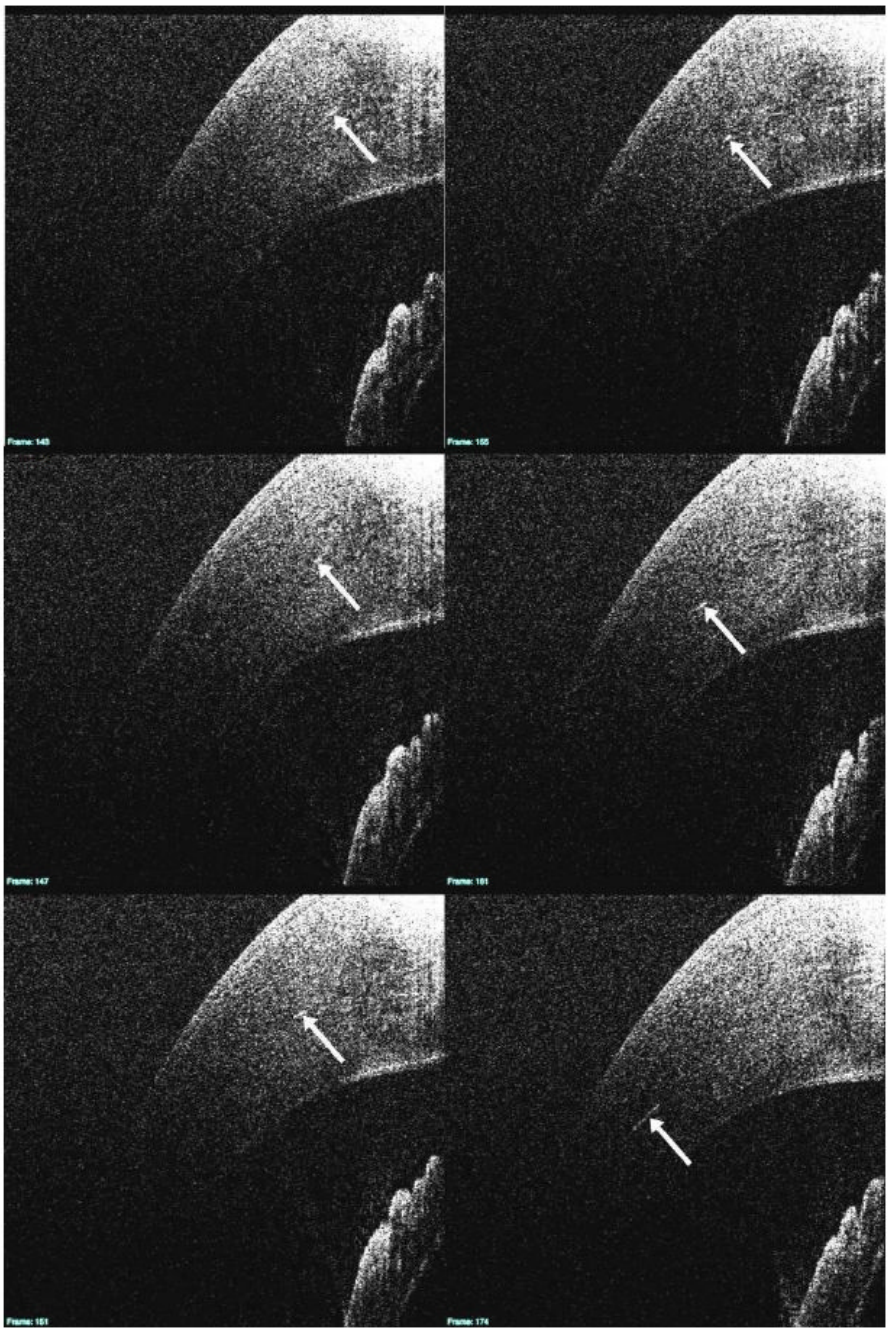

Fig. 7.

In this series of cross-sectional B-scan images, a number of hyper-reflective structures within the stroma are visible (white arrows). The 3D B-scan sequence is linked (View 1). In addition to the slices seen above, it also contains an en-face view of the cornea to the left of the slices.

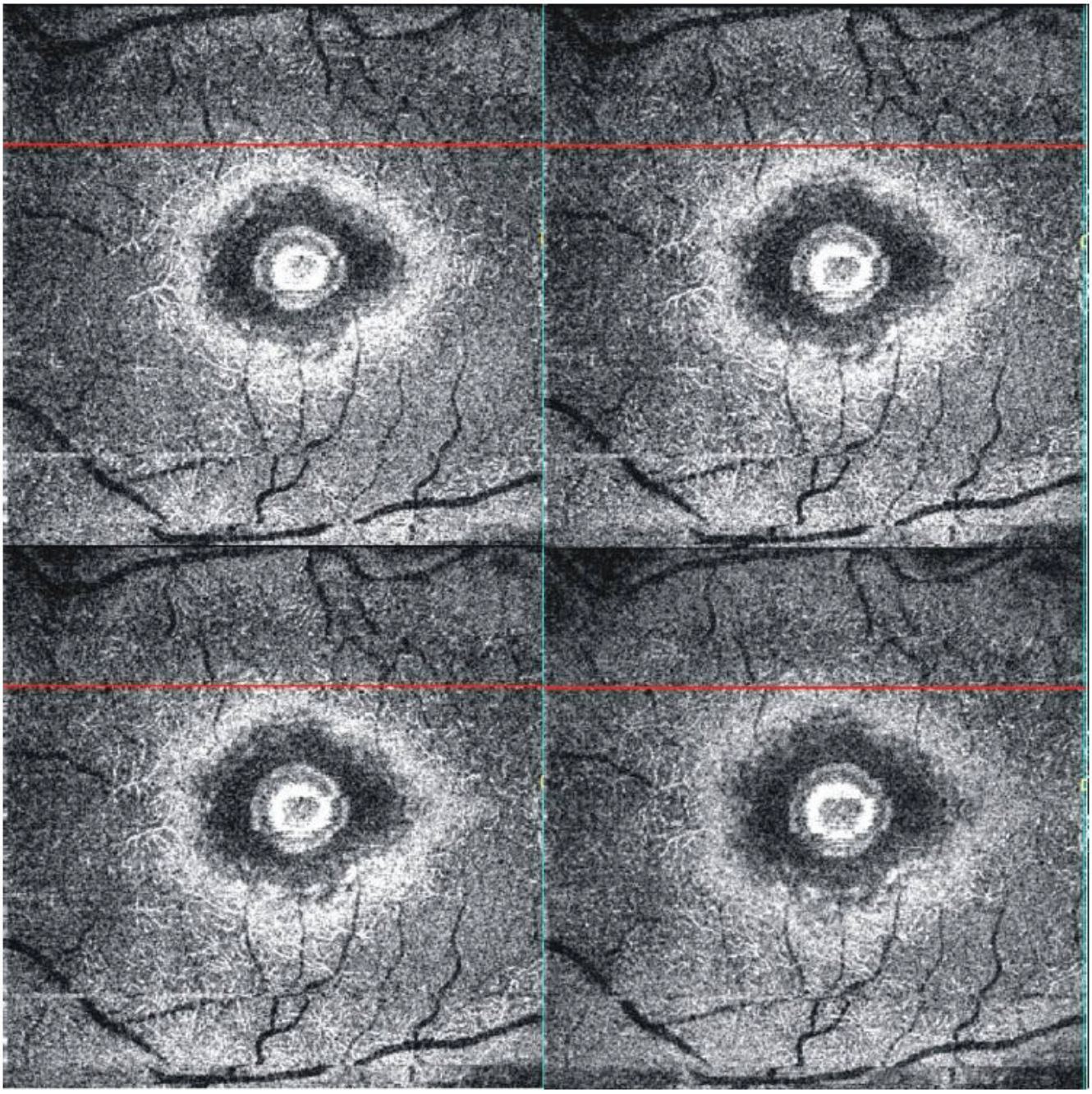

Fig. 8.
C-mode slab images of the outer plexiform layer of the perimacular retina review a detailed image of the retinal capillaries. Note that blood makes the capillaries appear white.

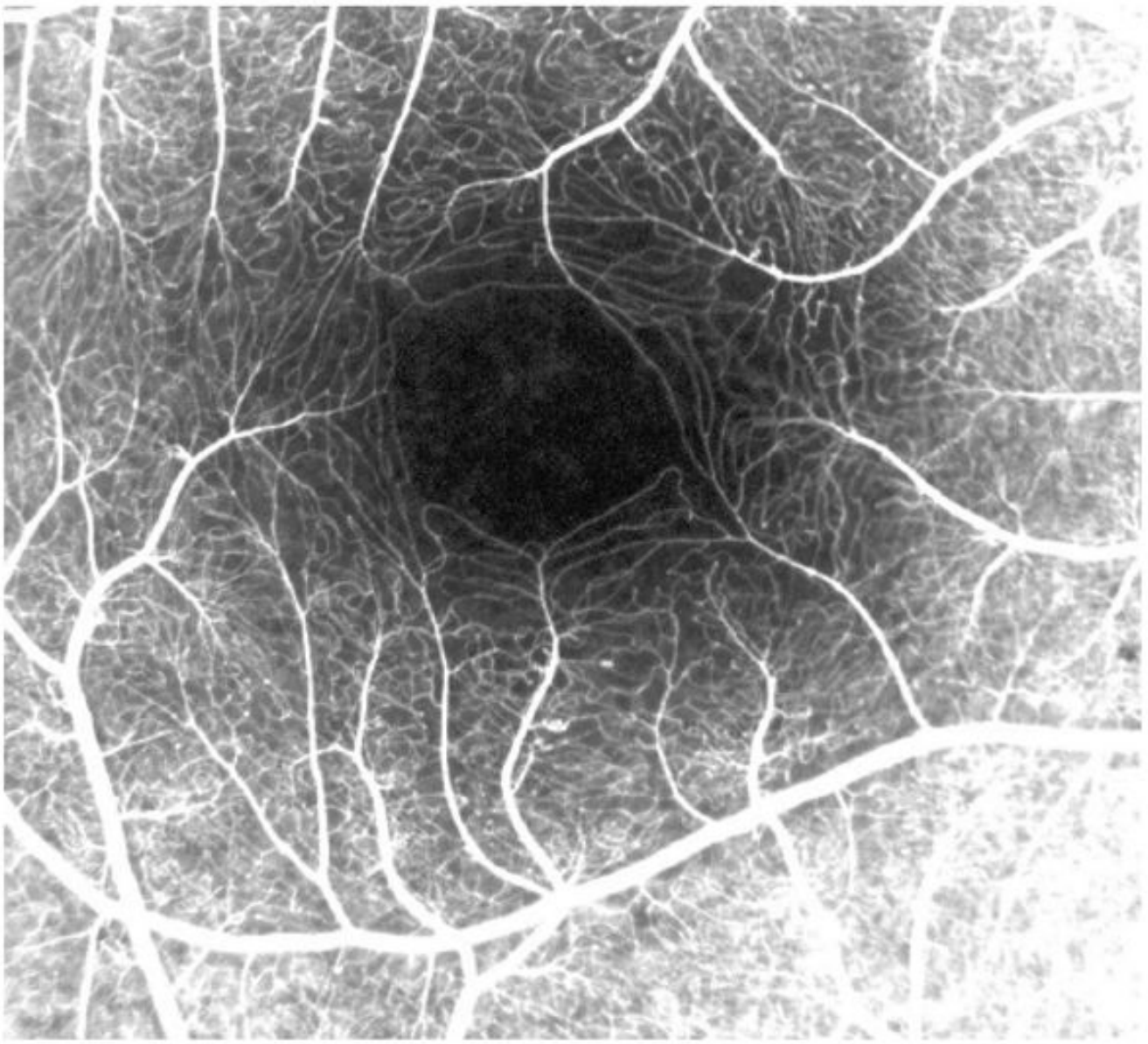

Fig. 9.
Macular capillaries visualized by fluorescein angiography.

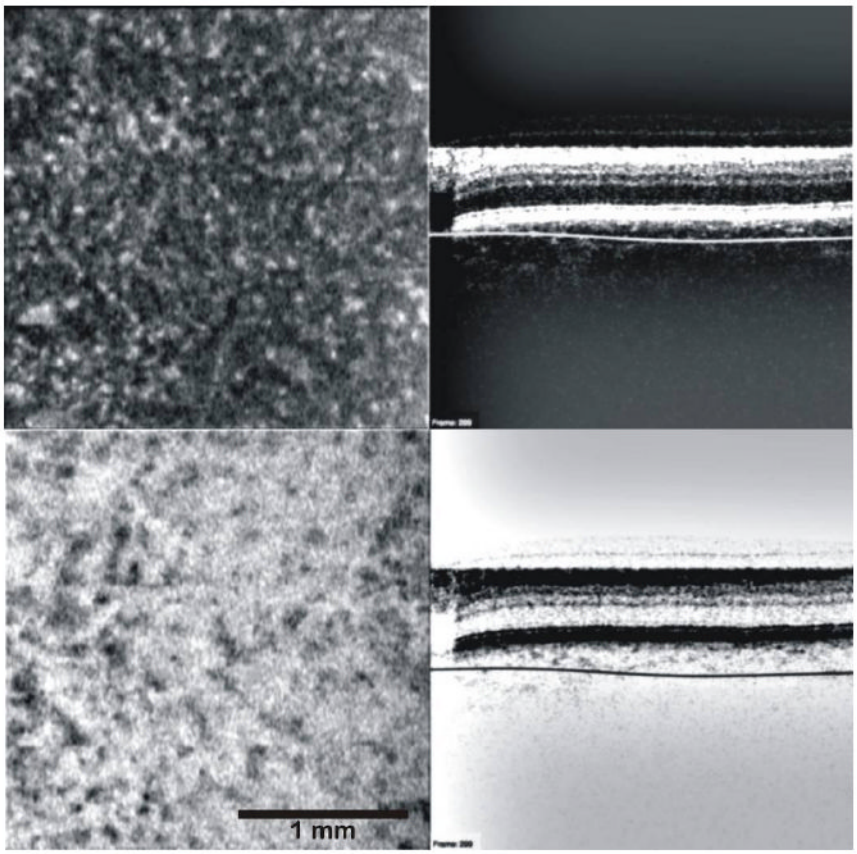

Fig. 10.

A C-mode slice below the retina (upper right) creates an image of the choriocapillaris (upper left). Inverting the image (black/white inversion, bottom) facilitates visualization of the vasculature (lower left, (View 2). The 3D C-mode sequence provides a fly-through view beginning at the posterior level of the photoreceptor/retinal pigment epithelium complex, and extending through the large vessels of the choroid. The images are black/white inverted, appearing similar to the lower left frame at the level of the choriocapillaris.

Fig. 11.

Pores in the lamina cribrosa (black spots, upper left) are clearly visible in a normal subject with a large disc (upper left). Note the enhanced visualization on the temporal side of the disc compared to the clinical view provided by the fundus photo on bottom. The C-mode slab is located in the lamina cribrosa/pre-lamina region of the optic nerve (upper right). The 3D dataset is presented as a C-mode sequence (View 3). The upper portion of this figure is one of the slices from the 3D dataset, with the stack of C-mode slices on the left, and the single frame repeated on the right.

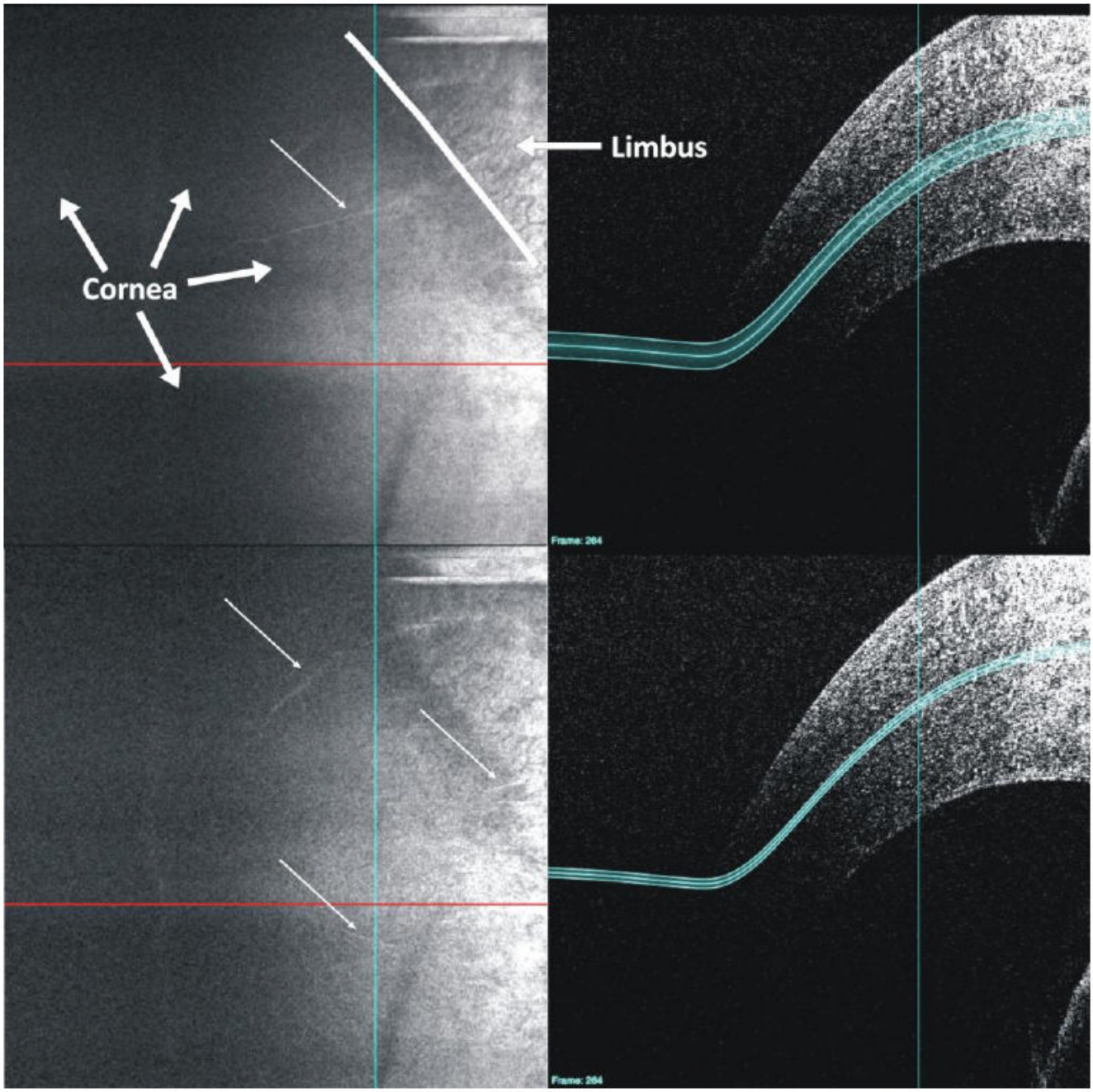

Fig. 12.

A customized C-mode slab positioned by hand along the curvature of the tissue reveals a continuous highly reflective structure extending from the limbus into the cornea (white arrows). The border between the cornea and limbus is marked with a white line in the upper left frame. Links are provided to both the B-scan (View 1) and C-mode (View 4) image sequences.